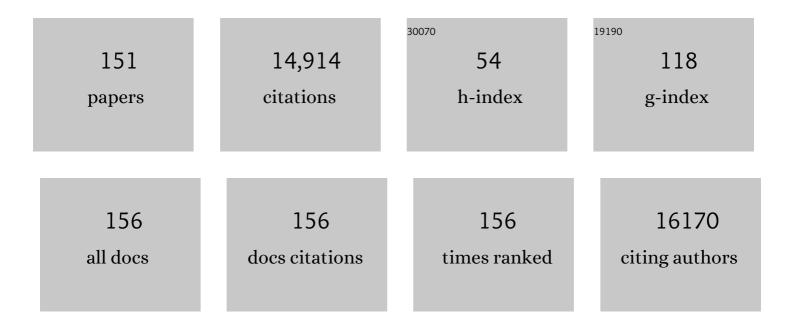
List of Publications by Year in descending order

Source: https://exaly.com/author-pdf/9040454/publications.pdf Version: 2024-02-01



KEVIN M RDINDLE

#	Article	IF	CITATIONS
1	A functional genomics strategy that uses metabolome data to reveal the phenotype of silent mutations. Nature Biotechnology, 2001, 19, 45-50.	17.5	948
2	The return of metabolism: biochemistry and physiology of the pentose phosphate pathway. Biological Reviews, 2015, 90, 927-963.	10.4	908
3	Detecting tumor response to treatment using hyperpolarized 13C magnetic resonance imaging and spectroscopy. Nature Medicine, 2007, 13, 1382-1387.	30.7	825
4	Magnetic resonance imaging of pH in vivo using hyperpolarized 13C-labelled bicarbonate. Nature, 2008, 453, 940-943.	27.8	796
5	Enhanced detection of circulating tumor DNA by fragment size analysis. Science Translational Medicine, 2018, 10, .	12.4	670
6	Analysis of Cancer Metabolism by Imaging Hyperpolarized Nuclei: Prospects for Translation to Clinical Research. Neoplasia, 2011, 13, 81-97.	5.3	623
7	Challenges to curing primary brain tumours. Nature Reviews Clinical Oncology, 2019, 16, 509-520.	27.6	540
8	Clinical Proton MR Spectroscopy in Central Nervous System Disorders. Radiology, 2014, 270, 658-679.	7.3	524
9	Non-invasive detection of apoptosis using magnetic resonance imaging and a targeted contrast agent. Nature Medicine, 2001, 7, 1241-1244.	30.7	513
10	New approaches for imaging tumour responses to treatment. Nature Reviews Cancer, 2008, 8, 94-107.	28.4	413
11	Production of hyperpolarized [1,4- ¹³ C ₂]malate from [1,4- ¹³ C ₂]fumarate is a marker of cell necrosis and treatment response in tumors. Proceedings of the National Academy of Sciences of the United States of America, 2009, 106, 19801-19806.	7.1	328
12	Hyperpolarized 13C MRI: Path to Clinical Translation in Oncology. Neoplasia, 2019, 21, 1-16.	5.3	316
13	Magnetic resonance imaging of tumor glycolysis using hyperpolarized 13C-labeled glucose. Nature Medicine, 2014, 20, 93-97.	30.7	298
14	Early detection of cancer. Science, 2022, 375, eaay9040.	12.6	291
15	Molecular imaging using fluorescent lectins permits rapid endoscopic identification of dysplasia in Barrett's esophagus. Nature Medicine, 2012, 18, 315-321.	30.7	285
16	Methodological consensus on clinical proton MRS of the brain: Review and recommendations. Magnetic Resonance in Medicine, 2019, 82, 527-550.	3.0	280
17	Tumor imaging using hyperpolarized ¹³ C magnetic resonance spectroscopy. Magnetic Resonance in Medicine, 2011, 66, 505-519.	3.0	229
18	Imaging Cell Death. Journal of Nuclear Medicine, 2014, 55, 1-4.	5.0	224

#	Article	IF	CITATIONS
19	Hyperpolarized [1- ¹³ C]-Ascorbic and Dehydroascorbic Acid: Vitamin C as a Probe for Imaging Redox Status in Vivo. Journal of the American Chemical Society, 2011, 133, 11795-11801.	13.7	177
20	Imaging Metabolism with Hyperpolarized ¹³ C-Labeled Cell Substrates. Journal of the American Chemical Society, 2015, 137, 6418-6427.	13.7	171
21	Detecting response of rat C6 glioma tumors to radiotherapy using hyperpolarized [1â€ ¹³ C]pyruvate and ¹³ C magnetic resonance spectroscopic imaging. Magnetic Resonance in Medicine, 2011, 65, 557-563.	3.0	152
22	¹³ C MR spectroscopy measurements of glutaminase activity in human hepatocellular carcinoma cells using hyperpolarized ¹³ Câ€labeled glutamine. Magnetic Resonance in Medicine, 2008, 60, 253-257.	3.0	148
23	Quantifying normal human brain metabolism using hyperpolarized [1–13C]pyruvate and magnetic resonance imaging. Neurolmage, 2019, 189, 171-179.	4.2	144
24	Imaging breast cancer using hyperpolarized carbon-13 MRI. Proceedings of the National Academy of Sciences of the United States of America, 2020, 117, 2092-2098.	7.1	138
25	Kinetic Modeling of Hyperpolarized 13C Label Exchange between Pyruvate and Lactate in Tumor Cells. Journal of Biological Chemistry, 2011, 286, 24572-24580.	3.4	133
26	The significance and mechanism of mitochondrial proton conductance. International Journal of Obesity, 1999, 23, S4-S11.	3.4	127
27	Detection of cellâ€free <scp>DNA</scp> fragmentation and copy number alterations in cerebrospinal fluid from glioma patients. EMBO Molecular Medicine, 2018, 10, .	6.9	123
28	Biomedical applications of hyperpolarized 13C magnetic resonance imaging. Progress in Nuclear Magnetic Resonance Spectroscopy, 2009, 55, 285-295.	7.5	121
29	ctDNA monitoring using patient-specific sequencing and integration of variant reads. Science Translational Medicine, 2020, 12, .	12.4	116
30	Artifactual uncoupling by uncoupling protein 3 in yeast mitochondria at the concentrations found in mouse and rat skeletal-muscle mitochondria. Biochemical Journal, 2002, 361, 49-56.	3.7	107
31	Magnetization transfer measurements of exchange between hyperpolarized [1- ¹³ C]pyruvate and [1- ¹³ C]lactate in a murine lymphoma. Magnetic Resonance in Medicine, 2010, 63, 872-880.	3.0	107
32	Noninvasive In Vivo Assessment of Cardiac Metabolism in the Healthy and Diabetic Human Heart Using Hyperpolarized ¹³ C MRI. Circulation Research, 2020, 126, 725-736.	4.5	105
33	A Comparison between Radiolabeled Fluorodeoxyglucose Uptake and Hyperpolarized 13C-Labeled Pyruvate Utilization as Methods for Detecting Tumor Response to Treatment. Neoplasia, 2009, 11, 574-IN11.	5.3	104
34	Magnetic resonance imaging with hyperpolarized [1,4- ¹³ C ₂]fumarate allows detection of early renal acute tubular necrosis. Proceedings of the National Academy of Sciences of the United States of America, 2012, 109, 13374-13379.	7.1	99
35	Direct Enhancement of Nuclear Singlet Order by Dynamic Nuclear Polarization. Journal of the American Chemical Society, 2012, 134, 7668-7671.	13.7	94
36	Imaging <scp>pH</scp> with hyperpolarized ¹³ C. NMR in Biomedicine, 2011, 24, 1006-1015.	2.8	93

#	Article	IF	CITATIONS
37	Dual-modality gene reporter for in vivo imaging. Proceedings of the National Academy of Sciences of the United States of America, 2014, 111, 415-420.	7.1	91
38	NMR methods for measuring enzyme kinetics in vivo. Progress in Nuclear Magnetic Resonance Spectroscopy, 1988, 20, 257-293.	7.5	89
39	A comparison of quantitative methods for clinical imaging with hyperpolarized ¹³ Câ€pyruvate. NMR in Biomedicine, 2016, 29, 387-399.	2.8	83
40	Imaging sialylated tumor cell glycans <i>in vivo</i> . FASEB Journal, 2011, 25, 2528-2537.	0.5	80
41	Metabolic Glycan Imaging by Isonitrile–Tetrazine Click Chemistry. ChemBioChem, 2013, 14, 1063-1067.	2.6	79
42	Detection of Cell Death in Tumors by Using MR Imaging and a Gadolinium-based Targeted Contrast Agent. Radiology, 2008, 246, 854-862.	7.3	78
43	Hyperpolarized 13C Spectroscopy Detects Early Changes in Tumor Vasculature and Metabolism after VEGF Neutralization. Cancer Research, 2012, 72, 854-864.	0.9	73
44	Measuring Tumor Glycolytic Flux in Vivo by Using Fast Deuterium MRI. Radiology, 2020, 294, 289-296.	7.3	73
45	Detection of Apoptosis Using the C2A Domain of Synaptotagmin I. Bioconjugate Chemistry, 2004, 15, 983-987.	3.6	72
46	Development and evaluation of new cyclooctynes for cell surface glycan imaging in cancer cells. Chemical Science, 2011, 2, 932.	7.4	71
47	MRI with hyperpolarised [1- ¹³ C]pyruvate detects advanced pancreatic preneoplasia prior to invasive disease in a mouse model. Gut, 2016, 65, 465-475.	12.1	71
48	Induction of apoptosis in two mammalian cell lines results in increased levels of fructose-1,6-Bisphosphate and CDP-choline as determined by31P MRS. Magnetic Resonance in Medicine, 1998, 40, 411-420.	3.0	69
49	Mitochondrial proton leak and the uncoupling proteins. Journal of Bioenergetics and Biomembranes, 1999, 31, 517-524.	2.3	68
50	Measurement of Plasma Cell-Free Mitochondrial Tumor DNA Improves Detection of Glioblastoma in Patient-Derived Orthotopic Xenograft Models. Cancer Research, 2019, 79, 220-230.	0.9	67
51	Detection of Tumor Response to a Vascular Disrupting Agent by Hyperpolarized 13C Magnetic Resonance Spectroscopy. Molecular Cancer Therapeutics, 2010, 9, 3278-3288.	4.1	66
52	Imaging Cell Surface Glycosylation in Vivo Using "Double Click―Chemistry. Bioconjugate Chemistry, 2013, 24, 934-941.	3.6	66
53	1H MRS-visible lipids accumulate during apoptosis of lymphoma cells in vitro and in vivo. Magnetic Resonance in Medicine, 2005, 54, 43-50.	3.0	65
54	MRI measurements of reporter-mediated increases in transmembrane water exchange enable detection of a gene reporter. Nature Biotechnology, 2017, 35, 75-80.	17.5	63

#	Article	IF	CITATIONS
55	Assessing responses to cancer therapy using molecular imaging. Biochimica Et Biophysica Acta: Reviews on Cancer, 2006, 1766, 242-261.	7.4	61
56	Fragmentation patterns and personalized sequencing of cellâ€free DNA in urine and plasma of glioma patients. EMBO Molecular Medicine, 2021, 13, e12881.	6.9	61
57	Comparison of the C2A Domain of Synaptotagmin-I and Annexin-V As Probes for Detecting Cell Death. Bioconjugate Chemistry, 2010, 21, 884-891.	3.6	57
58	Detection of tumor glutamate metabolism in vivo using ¹³ C magnetic resonance spectroscopy and hyperpolarized [1â€ ¹³ C]glutamate. Magnetic Resonance in Medicine, 2011, 66, 18-23.	3.0	55
59	Hyperpolarized singlet lifetimes of pyruvate in human blood and in the mouse. NMR in Biomedicine, 2013, 26, 1696-1704.	2.8	54
60	Brain Tumor Imaging. Journal of Clinical Oncology, 2017, 35, 2432-2438.	1.6	53
61	Hyperpolarized ¹³ C MRI and PET: In Vivo Tumor Biochemistry. Journal of Nuclear Medicine, 2011, 52, 1333-1336.	5.0	52
62	Probing Lactate Dehydrogenase Activity in Tumors by Measuring Hydrogen/Deuterium Exchange in Hyperpolarized <scp>l</scp> -[1- ¹³ C,U- ² H]Lactate. Journal of the American Chemical Society, 2012, 134, 4969-4977.	13.7	49
63	Dual-sugar imaging using isonitrile and azido-based click chemistries. Organic and Biomolecular Chemistry, 2013, 11, 7297.	2.8	49
64	Potential Clinical Roles for Metabolic Imaging with Hyperpolarized [1-13C]Pyruvate. Frontiers in Oncology, 2016, 6, 59.	2.8	49
65	Emerging Technologies to Image Tissue Metabolism. Cell Metabolism, 2019, 29, 518-538.	16.2	47
66	Analysis of image heterogeneity using 2D Minkowski functionals detects tumor responses to treatment. Magnetic Resonance in Medicine, 2014, 71, 402-410.	3.0	46
67	Spin echo measurements of the extravasation and tumor cell uptake of hyperpolarized [1―13 C]lactate and [1―13 C]pyruvate. Magnetic Resonance in Medicine, 2013, 70, 1200-1209.	3.0	45
68	Imaging Tumor Metabolism Using Positron Emission Tomography. Cancer Journal (Sudbury, Mass), 2015, 21, 129-136.	2.0	41
69	Imaging tumour cell metabolism using hyperpolarized 13C magnetic resonance spectroscopy. Biochemical Society Transactions, 2010, 38, 1220-1224.	3.4	40
70	Carbonic Anhydrase Activity Monitored <i>In Vivo</i> by Hyperpolarized 13C-Magnetic Resonance Spectroscopy Demonstrates Its Importance for pH Regulation in Tumors. Cancer Research, 2015, 75, 4109-4118.	0.9	40
71	Magnetic resonance imaging of cancer metabolism with hyperpolarized 13C-labeled cell metabolites. Current Opinion in Chemical Biology, 2018, 45, 187-194.	6.1	40
72	Hyperpolarized ¹³ C MRI of Tumor Metabolism Demonstrates Early Metabolic Response to Neoadjuvant Chemotherapy in Breast Cancer. Radiology Imaging Cancer, 2020, 2, e200017.	1.6	40

#	Article	IF	CITATIONS
73	Amplification of TRIM44: Pairing a Prognostic Target With Potential Therapeutic Strategy. Journal of the National Cancer Institute, 2014, 106, .	6.3	38
74	In vivo single-shot 13C spectroscopic imaging of hyperpolarized metabolites by spatiotemporal encoding. Journal of Magnetic Resonance, 2014, 240, 8-15.	2.1	38
75	Hyperpolarized [U- ² H, U- ¹³ C]Glucose reports on glycolytic and pentose phosphate pathway activity in EL4 tumors and glycolytic activity in yeast cells. Magnetic Resonance in Medicine, 2015, 74, 1543-1547.	3.0	38
76	Metabolic Imaging Detects Resistance to PI3Kα Inhibition Mediated by Persistent FOXM1 Expression in ER+ Breast Cancer. Cancer Cell, 2020, 38, 516-533.e9.	16.8	38
77	Dynamic ¹ H imaging of hyperpolarized [1â€ ¹³ C]lactate in vivo using a reverse INEPT experiment. Magnetic Resonance in Medicine, 2018, 79, 741-747.	3.0	37
78	Magnetic Resonance Imaging Is More Sensitive Than PET for Detecting Treatment-Induced Cell Death–Dependent Changes in Glycolysis. Cancer Research, 2019, 79, 3557-3569.	0.9	36
79	Analysis of heterogeneity in T2-weighted MR images can differentiate pseudoprogression from progression in glioblastoma. PLoS ONE, 2017, 12, e0176528.	2.5	34
80	Metabolic Imaging Detects Low Levels of Glycolytic Activity That Vary with Levels of c-Myc Expression in Patient-Derived Xenograft Models of Glioblastoma. Cancer Research, 2018, 78, 5408-5418.	0.9	34
81	Breast cancer–associated macrophages promote tumorigenesis by suppressing succinate dehydrogenase in tumor cells. Science Signaling, 2020, 13, .	3.6	34
82	Monitoring tumor cell death in murine tumor models using deuterium magnetic resonance spectroscopy and spectroscopic imaging. Proceedings of the National Academy of Sciences of the United States of America, 2021, 118, .	7.1	33
83	Assessing Oxidative Stress in Tumors by Measuring the Rate of Hyperpolarized [1-13C]Dehydroascorbic Acid Reduction Using 13C Magnetic Resonance Spectroscopy. Journal of Biological Chemistry, 2017, 292, 1737-1748.	3.4	32
84	Apoptosis detection using magnetic resonance imaging and spectroscopy. Progress in Nuclear Magnetic Resonance Spectroscopy, 2005, 47, 175-185.	7.5	31
85	Detection of transgene expression using hyperpolarized ¹³ C urea and diffusionâ€weighted magnetic resonance spectroscopy. Magnetic Resonance in Medicine, 2015, 73, 1401-1406.	3.0	31
86	Single shot threeâ€dimensional pulse sequence for hyperpolarized ¹³ C MRI. Magnetic Resonance in Medicine, 2017, 77, 740-752.	3.0	30
87	A Paramagnetic Nanoprobe To Detect Tumor Cell Death Using Magnetic Resonance Imaging. Nano Letters, 2007, 7, 1419-1423.	9.1	29
88	Imaging Mouse Cancer Models In Vivo Using Reporter Transgenes. Cold Spring Harbor Protocols, 2013, 2013, pdb.top069864.	0.3	29
89	Phosphorus-31 NMR measurements of the ADP concentration in yeast cells genetically modified to express creatine kinase. Biochemistry, 1990, 29, 3295-3302.	2.5	27
90	Oatp1 Enhances Bioluminescence by Acting as a Plasma Membrane Transporter for d-luciferin. Molecular Imaging and Biology, 2014, 16, 626-634.	2.6	27

#	Article	IF	CITATIONS
91	Hyperpolarised 13C-MRI identifies the emergence of a glycolytic cell population within intermediate-risk human prostate cancer. Nature Communications, 2022, 13, 466.	12.8	27
92	Mapping of oxygen tension and cell distribution in a hollow-fiber bioreactor using magnetic resonance imaging. , 1997, 56, 56-61.		26
93	Imaging Glycosylation In Vivo by Metabolic Labeling and Magnetic Resonance Imaging. Angewandte Chemie - International Edition, 2016, 55, 1286-1290.	13.8	26
94	Development of Timd2 as a reporter gene for MRI. Magnetic Resonance in Medicine, 2016, 75, 1697-1707.	3.0	26
95	Detection of apoptosis in tumors using magnetic resonance imaging and spectroscopy. Advances in Enzyme Regulation, 2002, 42, 101-112.	2.6	25
96	Optoacoustic Detection of Early Therapy-Induced Tumor Cell Death Using a Targeted Imaging Agent. Clinical Cancer Research, 2017, 23, 6893-6903.	7.0	25
97	Hyperpolarized Carbon-13 MRI for Early Response Assessment of Neoadjuvant Chemotherapy in Breast Cancer Patients. Cancer Research, 2021, 81, 6004-6017.	0.9	25
98	Measurement of bioreactor perfusion using dynamic contrast agent-enhanced magnetic resonance imaging. Biotechnology and Bioengineering, 2001, 75, 682-690.	3.3	24
99	Late Imaging with [1- ¹¹ C]Acetate Improves Detection of Tumor Fatty Acid Synthesis with PET. Journal of Nuclear Medicine, 2014, 55, 1144-1149.	5.0	24
100	Rapid Imaging of Tumor Cell Death In Vivo Using the C2A Domain of Synaptotagmin-I. Journal of Nuclear Medicine, 2017, 58, 881-887.	5.0	24
101	Tumor Cell-Derived Nitric Oxide Is Involved in the Immune-Rejection of an Immunogenic Murine Lymphoma. Cancer Research, 2004, 64, 152-161.	0.9	23
102	SPECT imaging of myocardial infarction using 99mTc-labeled C2A domain of synaptotagmin l in a porcine ischemia–reperfusion model. Nuclear Medicine and Biology, 2007, 34, 917-923.	0.6	23
103	Design and validation of a near-infrared fluorescence endoscope for detection of early esophageal malignancy. Journal of Biomedical Optics, 2016, 21, 084001.	2.6	23
104	Analysis of ¹³ C and ¹⁴ C labeling in pyruvate and lactate in tumor and blood of lymphomaâ€bearing mice injected with ¹³ C―and ¹⁴ Câ€ŀabeled pyruvate. NMR in Biomedicine, 2018, 31, e3901.	2.8	23
105	Imaging and â€`omic' methods for the molecular diagnosis of cancer. Expert Review of Molecular Diagnostics, 2010, 10, 417-434.	3.1	22
106	Expanding Theranostic Radiopharmaceuticals for Tumor Diagnosis and Therapy. Pharmaceuticals, 2022, 15, 13.	3.8	22
107	Spin echo proton NMR studies of the metabolism of malate and fumarate in human erythrocytes. Biochimica Et Biophysica Acta - Molecular Cell Research, 1982, 721, 191-200.	4.1	21
108	Characterization of image heterogeneity using 2D Minkowski functionals increases the sensitivity of detection of a targeted MRI contrast agent. Magnetic Resonance in Medicine, 2009, 61, 1218-1224.	3.0	21

#	Article	IF	CITATIONS
109	Versatile and enhanced tumour modelling in mice via somatic cell transduction. Journal of Pathology, 2014, 232, 449-457.	4.5	21
110	¹³ C magnetic resonance spectroscopic imaging of hyperpolarized [1― ¹³ C, U― ² H ₅] ethanol oxidation can be used to assess aldehyde dehydrogenase activity in vivo. Magnetic Resonance in Medicine, 2015, 73, 1733-1740.	3.0	21
111	Increased hyperpolarized [1â€ ¹³ C] lactate production in a model of joint inflammation is not accompanied by tissue acidosis as assessed using hyperpolarized ¹³ Câ€labelled bicarbonate. NMR in Biomedicine, 2018, 31, e3892.	2.8	21
112	Photogenerated Radical in Phenylglyoxylic Acid for in Vivo Hyperpolarized ¹³ C MR with Photosensitive Metabolic Substrates. Journal of the American Chemical Society, 2018, 140, 14455-14463.	13.7	21
113	[¹⁸ F]fluoroethyltyrosine-induced Cerenkov Luminescence Improves Image-Guided Surgical Resection of Glioma. Theranostics, 2018, 8, 3991-4002.	10.0	19
114	Following Metabolism in Living Microorganisms by Hyperpolarized ¹ H NMR. Journal of the American Chemical Society, 2016, 138, 12278-12286.	13.7	18
115	Effects of fasting on serial measurements of hyperpolarized [1― ¹³ C]pyruvate metabolism in tumors. NMR in Biomedicine, 2016, 29, 1048-1055.	2.8	18
116	Hyperpolarized 13C-Pyruvate Metabolism as a Surrogate for Tumor Grade and Poor Outcome in Renal Cell Carcinoma—A Proof of Principle Study. Cancers, 2022, 14, 335.	3.7	18
117	Hyperpolarized MRI, functional MRI, MR spectroscopy and CEST to provide metabolic information inAvivo. Current Opinion in Chemical Biology, 2021, 63, 209-218.	6.1	17
118	Imaging Glioblastoma Metabolism by Using Hyperpolarized [1- ¹³ C]Pyruvate Demonstrates Heterogeneity in Lactate Labeling: A Proof of Principle Study. Radiology Imaging Cancer, 2022, 4, .	1.6	17
119	Imaging Tumor Metabolism to Assess Disease Progression and Treatment Response. Clinical Cancer Research, 2016, 22, 5196-5203.	7.0	15
120	Quantitation of a spin polarizationâ€induced nuclear Overhauser effect (SPINOE) between a hyperpolarized 13 Câ€iabeled cell metabolite and water protons. Contrast Media and Molecular Imaging, 2014, 9, 182-186.	0.8	13
121	Analysis of CHO-K1 cell growth in a fixed bed bioreactor using magnetic resonance spectroscopy and imaging. , 1999, 30, 121-132.		12
122	³¹ P magnetization transfer measurements of P _i →ATP flux in exercising human muscle. Journal of Applied Physiology, 2016, 120, 649-656.	2.5	12
123	A referenceless Nyquist ghost correction workflow for echo planar imaging of hyperpolarized [1â€ ¹³ C]pyruvate and [1â€ ¹³ C]lactate. NMR in Biomedicine, 2018, 31, e3866.	2.8	12
124	Metabolomics: Pandora's Box or Aladdin's Cave?. Biochemist, 2003, 25, 15-17.	0.5	12
125	Investigating the Performance of Intensive Mammalian Cell Bioreactor Systems Using Magnetic Resonance Imaging and Spectroscopy. Biotechnology and Genetic Engineering Reviews, 1998, 15, 499-520.	6.2	11
126	Hyperpolarized ¹³ C spectroscopic imaging using singleâ€shot 3D sequences with unpaired adiabatic refocusing pulses. NMR in Biomedicine, 2018, 31, e4004.	2.8	11

#	Article	IF	CITATIONS
127	³¹ P NMR measurements of the effects of unsaturated fatty acids on cellular phospholipid metabolism. Magnetic Resonance in Medicine, 1996, 35, 481-488.	3.0	10
128	Probing hepatic metabolism of [2-13C]dihydroxyacetone in vivo with 1H-decoupled hyperpolarized 13C-MR. Magnetic Resonance Materials in Physics, Biology, and Medicine, 2021, 34, 49-56.	2.0	10
129	Comparison of 13 C MRI of hyperpolarized [1―13 C]pyruvate and lactate with the corresponding mass spectrometry images in a murine lymphoma model. Magnetic Resonance in Medicine, 2021, 85, 3027-3035.	3.0	9
130	Imaging Glycosylation In Vivo by Metabolic Labeling and Magnetic Resonance Imaging. Angewandte Chemie, 2016, 128, 1308-1312.	2.0	8
131	¹³ C magnetic resonance spectroscopy measurements with hyperpolarized [1― ¹³ C] pyruvate can be used to detect the expression of transgenic pyruvate decarboxylase activity in vivo. Magnetic Resonance in Medicine, 2016, 76, 391-401.	3.0	8
132	Subâ€minute kinetics of human red cell fumarase: ¹ H spinâ€echo NMR spectroscopy and ¹³ C rapidâ€dissolution dynamic nuclear polarization. NMR in Biomedicine, 2018, 31, e3870.	2.8	8
133	Glyoxalase activity in human erythrocytes and mouse lymphoma, liver and brain probed with hyperpolarized 13C-methylglyoxal. Communications Biology, 2018, 1, 232.	4.4	8
134	Deuterium MRSI of tumor cell death in vivo following oralÂdelivery of <scp>²H</scp> ″abeled fumarate. Magnetic Resonance in Medicine, 2022, 88, 2014-2020.	3.0	8
135	Studies of metabolic control using NMR and molecular genetics. Journal of Molecular Recognition, 1997, 10, 182-187.	2.1	7
136	18F-C2Am: a targeted imaging agent for detecting tumor cell death in vivo using positron emission tomography. EJNMMI Research, 2020, 10, 151.	2.5	7
137	Dynamic nuclear polarisation: The future of imaging in oncology?. Porto Biomedical Journal, 2017, 2, 71-75.	1.0	5
138	A multi spin echo pulse sequence with optimized excitation pulses and a 3D cone readout for hyperpolarized 13 C imaging. Magnetic Resonance in Medicine, 2020, 84, 1895-1908.	3.0	5
139	Increasing the sensitivity of hyperpolarized [15 N 2]urea detection by serial transfer of polarization to spinâ€coupled protons. Magnetic Resonance in Medicine, 2020, 84, 1844-1856.	3.0	5
140	Enzymologyin vivo using NMR and molecular genetics. Journal of Molecular Recognition, 1993, 6, 159-165.	2.1	4
141	Genetic algorithmâ€based optimization of pulse sequences. Magnetic Resonance in Medicine, 2022, 87, 2130-2144.	3.0	4
142	Spectroscopic measurements of metabolic fluxes. Nature Biomedical Engineering, 2020, 4, 254-256.	22.5	3
143	Multi-modal imaging of high-risk ductal carcinoma in situ of the breast using C2Am: a targeted cell death imaging agent. Breast Cancer Research, 2021, 23, 25.	5.0	3
144	Editorial commentary for the special issue: technological developments in hyperpolarized 13C imaging—toward a deeper understanding of tumor metabolism in vivo. Magnetic Resonance Materials in Physics, Biology, and Medicine, 2021, 34, 1-3.	2.0	3

9

#	Article	IF	CITATIONS
145	Gene reporters for magnetic resonance imaging. Trends in Genetics, 2022, 38, 996-998.	6.7	3
146	Metabolic imaging with hyperpolarized [1-13C] pyruvate in patient-derived preclinical mouse models of breast cancer. STAR Protocols, 2021, 2, 100608.	1.2	2
147	Mapping of oxygen tension and cell distribution in a hollowâ€fiber bioreactor using magnetic resonance imaging. Biotechnology and Bioengineering, 1997, 56, 56-61.	3.3	1
148	Analysis of metabolic controlIn Vivousing molecular genetics. Cell Biochemistry and Function, 1996, 14, 269-276.	2.9	0
149	Rücktitelbild: Imaging Glycosylation In Vivo by Metabolic Labeling and Magnetic Resonance Imaging (Angew. Chem. 4/2016). Angewandte Chemie, 2016, 128, 1592-1592.	2.0	0
150	Frontispiece: Siteâ€6elective Modification of Proteins with Oxetanes. Chemistry - A European Journal, 2017, 23, .	3.3	0
151	Innovating Metabolic Biomarkers for Hyperpolarized NMR. , 2021, , 151-179.		Ο